

Anisotropic Diffusion Limited Aggregation in three dimensions - universality and non-universality.

Nicholas R. Goold,^{1,*} Ellák Somfai,^{1,2,†} and Robin C. Ball^{1,‡}

¹*Department of Physics, University of Warwick, Coventry CV4 7AL, United Kingdom*

²*Universiteit Leiden, Instituut-Lorentz, PO Box 9506, 2300 RA Leiden, The Netherlands*

(Dated: September 21, 2018)

We explore the macroscopic consequences of lattice anisotropy for Diffusion Limited Aggregation (DLA) in three dimensions. Simple cubic and BCC lattice growths are shown to approach universal asymptotic states in a coherent fashion, and the approach is accelerated by the use of noise reduction. These states are strikingly anisotropic dendrites with a rich hierarchy of structure. For growth on an FCC lattice, our data suggest at least two stable fixed points of anisotropy, one matching the BCC case. Hexagonal growths, favouring six planar and two polar directions, appear to approach a line of asymptotic states with continuously tunable polar anisotropy. The more planar of these growths visually resemble real snowflake morphologies.

Our simulations use a new and dimension-independent implementation of the Diffusion Limited Aggregation (DLA) model. The algorithm maintains a hierarchy of sphere-coverings of the growth, supporting efficient random walks onto the growth by spherical moves. Anisotropy was introduced by restricting growth to certain preferred directions.

PACS numbers: 61.43.Hv

I. INTRODUCTION

The Diffusion Limited Aggregation (DLA) [1] model has been the focus of a great deal of research due both to the fractal [2, 3, 4] and multifractal [5, 6, 7] properties of the clusters it produces, and to its underlying mathematical connection to diverse problems including solidification [8, 9], viscous fingering [10] and electrodeposition [11, 12]. Its key feature is that the surface irreversibly absorbs an incident diffusive flux, and growth velocity is locally proportional to that flux density.

The problem is mathematically ill-posed unless the growth is constrained to remain smooth below some “ultra-violet cut-off” lengthscale, which in most simulation studies has been supplied by a particle size or lattice scale. Experimentally the cut-off scale can be more subtle, for example in solidification regulated by surface tension it varies with the local incident flux density raised to power $-m$, with $m = 1/2$. Interest has also focussed on the more general Dielectric Breakdown Model [13] cases where growth velocity is proportional to the incident diffusive flux raised to some power η . Tuning η has been claimed to match appearance between DBM growths (albeit in two dimensions) and real snowflakes [14]. Recent theory [15, 16] suggests quantitative equivalence classes exist in the η, m plane, so that for example solidification should have a simpler-to-simulate equivalent at fixed cut-off ($m = 0$) at the computational expense of non-trivial $\eta \neq 1$.

A feature of real solidification patterns is that they

macroscopically strongly favour growth in specific directions, corresponding to microscopic crystal lattice directions. The tendency of snow crystals to grow six arms is well known, and lately this has been replicated in controlled laboratory studies [17]. Cubic crystalline anisotropy also produces striking anisotropic “dendrite” growth: succinonitryl is the classical example [18, 19], and lately colloidal crystal exemplars have been observed in growth under microgravity [20, 21].

The manner in which surface tension and its anisotropy select the morphology of growing tips has been the subject of intense analytical study [22]. Full numerical simulations of the continuum growth equations have confirmed the theory and extended the spatial range out to growths with significant side-branching [23, 24], but none of these studies could claim to reach the asymptotic regime of fractal growth.

Simple lattice and particle based simulations differ by having fixed cut-off scale and lacking realistic local detail, but they can reveal the limiting behaviour of highly branched growth. In two dimensions a range of different angular anisotropies have been shown to be relevant both by theory [25, 26] and through simulations yielding self-similar dendritic morphologies. Our principle objective in this paper is to deliver the same level of understanding for three-dimensional simulations, which have not been systematically explored in the literature to date.

We first introduce a new implementation of the DLA model that involves enclosing the aggregates with a series of coverings, each made up of a set of spheres, and show that it can successfully grow large, three-dimensional DLA clusters. This algorithm entails no intrinsic lattice or orientational bias, giving us a well posed isotropic reference.

We then show how anisotropy can be introduced to the algorithm by confining growth to certain preferred direc-

*Electronic address: N.R.Goold@warwick.ac.uk

†Electronic address: ellak@lorentz.leidenuniv.nl

‡Electronic address: r.c.ball@warwick.ac.uk

tions, and combine this with a noise reduction technique in which growth is only permitted after $H \geq 1$ random walkers have hit a growth site on the cluster. We characterise growths using anisotropy functions which are sensitive to the growth of fingers along the possible favoured directions. We present a systematic comparison of the evolution of growths within cubic symmetry, in particular the respective cases where growth is favoured along the nearest neighbour directions of one of the simple cubic, body-centred cubic and face-centred cubic lattices. We also study growth with uniaxial bias, where growth in polar and planar directions are inequivalently favoured, particularly including the three dimensional hexagonal lattice.

We show that SC and BCC aggregates approach universal, anisotropic asymptotic states independent of the level of noise reduction, and that the approach to each of these states follows a single mastercurve. FCC anisotropy is much slower to emerge, and we show that while high noise reduction clusters appear to approach an anisotropic fixed point in the same fashion, the existence of a different fixed point(s) for low noise reduction growths cannot be ruled out. For growth with uniaxial bias, we observe limiting polar-to-planar aspect ratios of the clusters which depend continuously on the level of input bias. Thus for the three dimensional hexagonal lattice there appears to be a tunable continuum of asymptotic states.

II. GROWTH ALGORITHM

The original DLA algorithm takes as its starting point a single fixed seed particle. A random walker is released from some distance away and diffuses freely until it hits the seed, at which point it sticks irreversibly. Further particles are released one at a time and a fractal cluster is formed. Early simulations were done on (mostly cubic) lattices, since this reduced the computer run-time required, and cluster sizes were limited to $N \simeq 10^4$ particles.

Modern DLA simulations are performed off-lattice and use a number of tricks to speed up the growth. Since a diffusing particle should reach the aggregate from a random direction, each walker can be released from a randomly chosen point on a sphere that just encloses the cluster. When a walker is far from the cluster it is allowed to take larger steps than when it is nearby, as long as it never takes a step larger than the distance to the nearest point of the cluster. A major development was the Brady-Ball algorithm [27], which involves covering the cluster with a series of coarse “mappings”, to give a lower bound on the distance to the cluster without looking up the position of every cluster particle. A further refinement was invented by Tolman and Meakin [28], whereby the coarse mappings cover the cluster in a manner constrained to give a margin of safety: this enables much simpler (e.g. spherical) moves to be taken. Cluster

sizes of $N \simeq 10^7$ are easily obtainable by these methods.

Our new algorithm is a fundamentally off-lattice and dimension independent development of the Brady-Ball-Tolman-Meakin algorithm. We represent the cluster in terms of a set of *zeroth level* spheres, and we maintain a hierarchy of coarser scale sphere coverings of these labelled by higher levels. For simplicity of exposition, we describe the case where the physical cluster particles are monodisperse, in which case it is convenient to choose the radius r_0 of the zeroth level spheres to correspond to the centre-to-centre distance between contacting particles (“sticking diameter”).

Higher level coverings, $n > 0$, each consist of a set of spheres of radius r_n such that every zeroth level sphere is *safely* covered, in the following sense: all points within distance ϕr_n of (the surface of) every zeroth level sphere lie inside the covering. Each covering is also *simply* contained by all higher level coverings. To make this structure easier to maintain we further required that each zeroth level sphere was safely covered by a single (not necessarily unique) sphere at all levels $n > 0$. We chose the coverings to have a geometric progression of size, with $r_n = \epsilon^{1-n} r_1$, and terminated the hierarchy when safe covering of the whole cluster was achieved by a single sphere.

Each sphere at level $n > 0$ carries a full set of *downlinks*. These consist of a pointer to every “child” sphere at level $n - 1$ which overlaps the parent. In addition we gave each sphere (below the highest level) one *uplink*, pointing to one of its parents; this is only required for the random walks (see later for choice).

This construction gives an efficient method of generating moves for our random walkers. At each step we need only determine the highest level covering that the walker is outside to give a lower bound on the walker’s distance from the cluster. This in turn entails tracking one (generally not unique) “enclosing” sphere which the walker does lie inside at the next level up.

Given that the walker lies inside an enclosing sphere at level m but outside the lower coverings, we first determine the nearest distance d from the walker to either the enclosing sphere or any of its children. The walker can then make a spherically distributed move of distance $d + \phi r_{m-1}$, because the nearest point of the cluster must be at least this far away. If the walker has moved outside the previous enclosing sphere, we follow uplinks until we find a new enclosing sphere. We then recursively replace that sphere by any of its children which enclose the walker, until a lowest level enclosing sphere is found as required for the next move of the walker.

Walkers are deemed to have hit the cluster when they find themselves inside a cluster particle. They are constrained by a (very small) minimum step size, typically $10^{-3} r_0$, so they can only ever trespass this far into the cluster. They are then “backed up” to the cluster perimeter and added to the aggregate.

As new particles are added to the cluster we must check that they are safely covered at each level $n > 0$. We start

at the maximum level, and create new maximum levels above it if required. Then we move down levels to $n = 1$ checking for safe coverage at each, noting the sphere that provided this. A level n sphere that safely covers our new site will necessarily overlap that which did so at the previous level $n + 1$, so the the search at each level can be restricted to the children of the previous safe container. If none of these give safe coverage we must add a new sphere at level n , ensuring that the integrity of the data structure is maintained and all the required new links are put in place.

The safe container at level $n + 1$ is made the parent of the new sphere at level n ; this is the uplink used by our random walkers. The new sphere could simply be centred on the particle we wish to add; however, in an attempt to maximise the efficiency of our coverings we offset the new sphere by a distance γr_n in the direction of local growth. This offset is constrained by our safe coverage requirement to obey $r_0 + \gamma r_n + \phi r_n < r_n$, which is most severe for $n = 1$ leading to

$$r_1(1 - \gamma - \phi) > r_0. \quad (1)$$

We must now find all the spheres which may need a downlink to or from the new sphere. To facilitate this we impose that each level covering is simply (but with no required margin) contained within those above it. In terms of our parameters this requires $r_n(1 + \gamma) < \phi r_{n+1} + r_0$ and choosing a geometric progression of radii $r_n = r_1/\epsilon^{n-1}$ with $\epsilon < 1$ and no limit on n then requires

$$1 + \gamma < \frac{\phi}{\epsilon}. \quad (2)$$

This constraint ensures that our new sphere is completely covered by the level $n + 2$ safe container, whose child list will hence contain all the level $n + 1$ spheres that need linking to the new sphere. Similarly, our new sphere is also covered by the level $n + 1$ safe container, and so any level $n - 1$ spheres to which the new sphere needs downlinks are guaranteed to be children of the children of that safe container. Thus by remembering the spheres which provided safe coverage at the previous two levels and selecting parameter values subject to the constraints (1) and (2) we can insert all the necessary new links, and ensure the integrity of our data structure remains intact as the cluster growth proceeds.

Taking $r_0 = 1$ for convenience, a somewhat ad-hoc optimisation scheme suggested the following parameters to minimise the run-time of our program in three dimensions: $r_1 = 2.1$, $\gamma = 0.29$, $\phi = 0.4$ and $\epsilon = 0.3$. We observe that the order of the algorithm is close to linear in N , consistent with the earlier discussion of Ball and Brady [27]. Figure 1 shows a large off-lattice DLA cluster grown in three dimensions by the new scheme and the convergence of measured fractal dimension D_f to a value ~ 2.5 , in good agreement with previous simulations [28, 29].

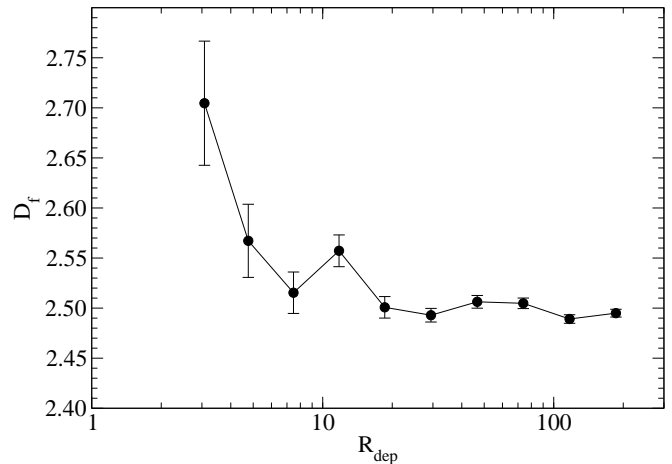
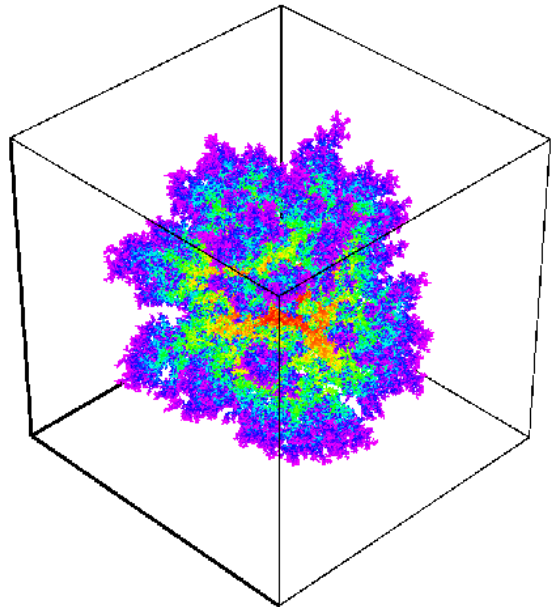


FIG. 1: (Color online) A three-dimensional DLA cluster grown using the new algorithm containing $N = 10^6$ particles, and the fractal dimension D_f plotted against the deposition radius R_{dep} obtained by averaging over a sample of 100 such clusters. D_f converges to a value of ~ 2.5 in agreement with previous results.

III. ANISOTROPY AND NOISE REDUCTION

We introduce anisotropy to our simulations by restricting growth to a set of preferred directions, effectively growing our clusters on a lattice. When a cluster site is “grown” (see following), we add new “sticky sites” of prospective growth offset from the grown site in each of our lattice directions. Sticky sites in turn grow when they have accreted a set threshold number of walkers $H \geq 1$. Requiring $H > 1$ walkers for growth gives better averaging over the diffusion field, amounting to a noise reduction. Noise reduction has been widely used for on-lattice planar DLA simulations [30], where it was found

TABLE I: Values of anisotropy functions A_4 and A_6 for growth along the nearest neighbour directions of simple, body-centred and face-centred cubic lattices.

	Simple Cubic	Body-centred Cubic	Face-centred Cubic
A_4	1	-2/3	-1/4
A_6	-8/13	-128/117	1

to considerably accelerate the approach to asymptotic morphology.

We have grown aggregates favouring growth in the local simple, body-centred and face-centred cubic lattice directions. To characterise the macroscopic anisotropy of a resulting N -particle cluster we use functions $A_K = \frac{1}{N} \sum_{i=1}^N a_K(x_i, y_i, z_i)$, where (x_i, y_i, z_i) are the coordinates of the i th particle relative to the seed of the growth, and a_K is a function with maxima in the appropriate lattice directions. We have constructed a_K out of angular harmonics of order K , with the appropriate symmetry and minimal order to distinguish the different lattice responses of study.

Growth biased to the direction of simple cubic axes (relative to the cluster seed) is detected by using a harmonic of order 4,

$$a_4 = \frac{5}{2r^4} (x^4 + y^4 + z^4) - \frac{3}{2},$$

where $r^2 = x^2 + y^2 + z^2$ and the normalisation is chosen such that $A_4 = 1$ for growth exactly along the lattice axes. Likewise growth along the nearest neighbour directions of an FCC lattice gives $A_6 = 1$ based on

$$a_6 = \frac{112}{13r^6} (x^6 + y^6 + z^6 + \frac{15}{4} (x^4y^2 + x^2y^4 + x^4z^2 + x^2z^4 + y^4z^2 + y^2z^4)) - \frac{120}{13}.$$

The combination of these two enables us to distinguish by sign growth along SC, BCC or FCC directions as summarised in Table I, where values given are for the extreme case of growth confined to the corresponding nearest neighbour directions from the central seed.

We have also grown aggregates favouring six planar and two polar directions of growth. These growths have their polar directions inequivalent (by any symmetry) to their planar ones so we were naturally led to admit different values of noise reduction in the two classes of local growth direction to tune their relative growth. We found the clearest characterisation of the corresponding growth response of these clusters simply by measuring their aspect ratios, which we calculate using extremal radii. We define a cluster's aspect ratio as z_{\max}/x_{\max} , or, in terms of crystallographic notation, c/a .

IV. RESULTS

We grew aggregates favouring SC, BCC and FCC lattice directions at several levels of noise reduction H from 1 to 100, and measured their response using our anisotropy functions A_K . The clusters were grown to size $N = 3.16 \times 10^4$ particles, where a site was included in this tally only when it had been hit H times.

Figure 2 shows example SC and BCC clusters grown at the highest level of noise reduction $H = 100$. Both clusters have major arms in the appropriate lattice directions, and each arm exhibits secondary growth along the remaining favoured directions.

The measured anisotropy A_4 for SC and BCC growths at various H is shown in Figure 3. Both sets of clusters appear to approach universal asymptotic values of A_4 independent of noise reduction: $A_4(\infty) \simeq 0.65$ for SC growths and $A_4(\infty) \simeq -0.5$ for BCC growths. These values can be approached from both above and below, depending on H .

The consistency of the shapes of the anisotropy curves suggest that for these types of growth there may exist “mastercurves” that embody the evolution of A_4 towards its asymptotic value, as a function of rescaled N . All individual curves, regardless of H , will lie somewhere on these mastercurves. To test this hypothesis for each case we shifted the curves along the N -axis by a factor $k(H)$ until, by eye, they appeared to follow a single curve. Figure 4(a) and (b) shows the results of this procedure for both the SC and BCC growths. For each case, we have used only the results for $N > 10^2$ in order to be sure of the correct general trend, and we could not use the very low H curves because they vary too little across the simulation range to give sufficient vertical overlap. The figure shows power law relationships between the noise reduction H and the shift factors $k(H)$ in both cases, further evidence that this mastercurve approach correctly describes the evolution of SC and BCC growths.

In the SC case, Figure 4(a), the shifted curves for values of H from 3 to 16 are shown. For $H > 16$, since the anisotropy curves are very close to the asymptotic value of A_4 and are hence very flat, this curve-shifting process fails. There presumably exists some ideal noise reduction value H^* for which the A_4 curve will approach the asymptote most quickly, and we would of course expect the power law scaling to break down as H approaches this value. The curves for very high values $H \geq 28$ approach the asymptotic value from above, and it should presumably be possible to map them onto a second mastercurve. However to test that systematically would require more data of considerable computational cost.

For the BCC case, Figure 4(b), the anisotropy is much slower to emerge from the noise and the curves for all values of H save the very highest $H = 100$ approach the asymptotic value from the same direction, and the mastercurve includes all values of H from 5 to 24. Above $H = 24$, the procedure fails in the same fashion as the SC case as H^* is approached.

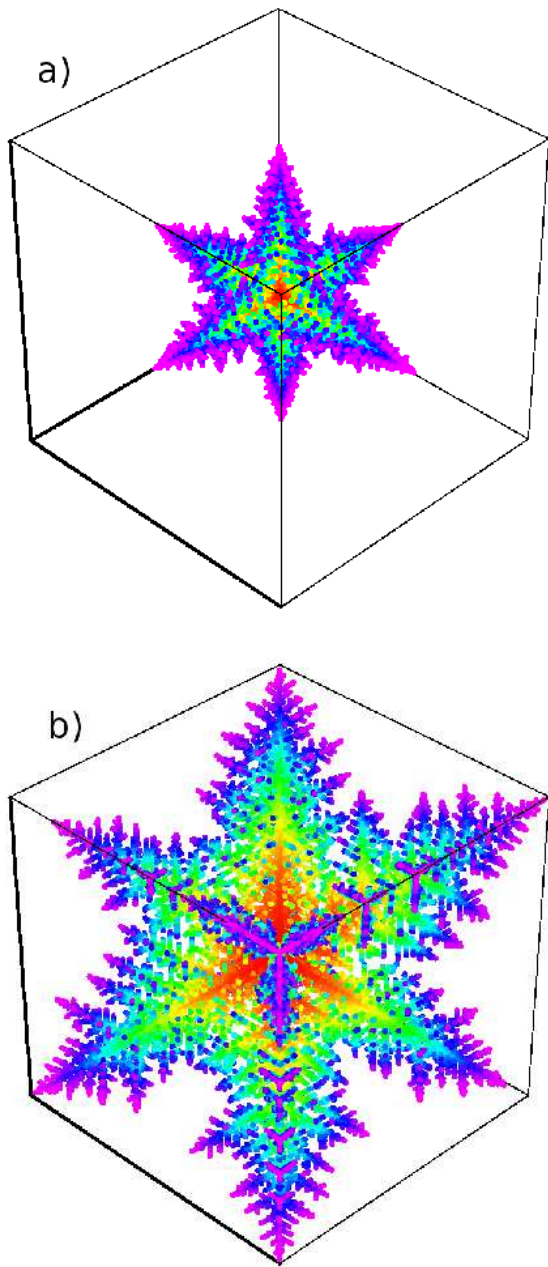


FIG. 2: (Color online) Anisotropic DLA clusters grown by the new method: **a)** simple cubic case, and **b)** body-centred cubic case. Each contains 3.16×10^4 sites, grown under noise reduction such that sites were grown after capturing $H = 100$ walkers.

Anisotropy curves A_6 for FCC growths are shown in Figure 5(a), and it is immediately apparent that their behaviour is not as straightforward as the SC and BCC cases. For high H growths, A_6 appears to be increasing in a fashion similar to that previously observed, suggesting the existence of a fixed point of anisotropy for FCC growth at $A_6(\infty) \simeq 0.48$. All the curves approach this value from below, suggesting that the FCC anisotropy is

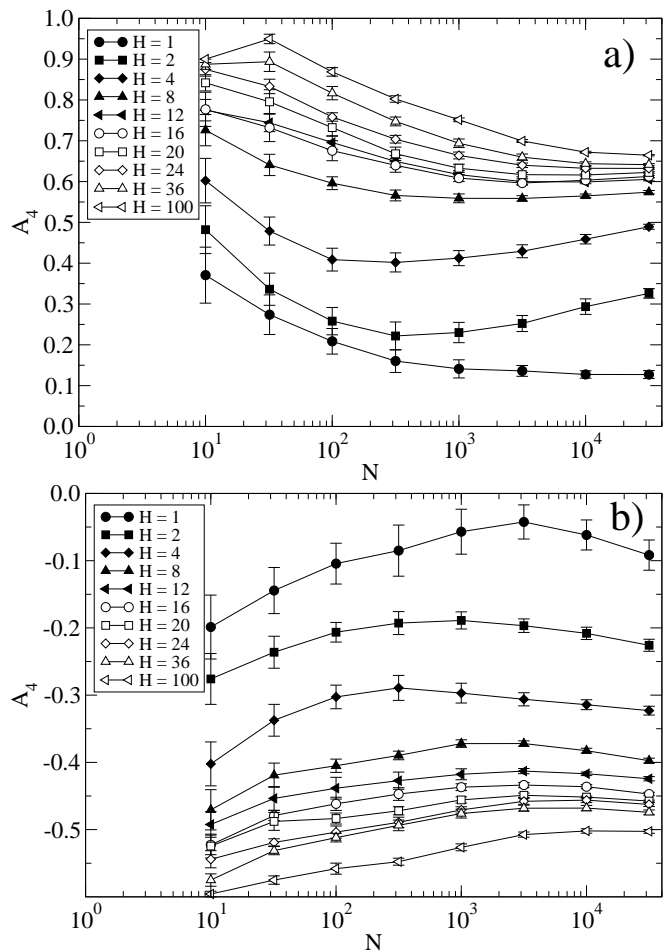


FIG. 3: Anisotropy function A_4 evaluated for **a)** simple cubic and **b)** body-centred cubic growths at various levels of noise reduction H as a function of the number of sites grown N . Each curve is based on the average over 10 clusters. Comparing to reference values in Table I, these confirm quantitatively the visual impression from Figure 2 that the respective SC and BCC anisotropies are self-sustaining under growth.

much slower to emerge from the noise than the SC and BCC anisotropies. This seems reasonable given that the FCC anisotropy has more competing “arms” than the other growths, and we have verified that the $H = 100$ clusters do indeed appear to have a full set of 12 arms. A mastercurve for these higher values of H is shown in Figure 5(b), and seems to describe these results well.

For low noise reduction clusters $H < 8$ however, A_6 does not increase over the course of the growth, and if anything appears to be *decreasing* at large N towards a value of about zero, suggesting the possible existence of another fixed point. Visualisations of these low H FCC clusters appeared to indicate some growth along the BCC lattice directions; Figure 6 shows an example of this for a low noise reduction $H = 6$ cluster, and for comparison a high noise reduction $H = 100$ cluster exhibiting some growth in all 12 FCC lattice directions.

We were hence led to apply the BCC anisotropy func-

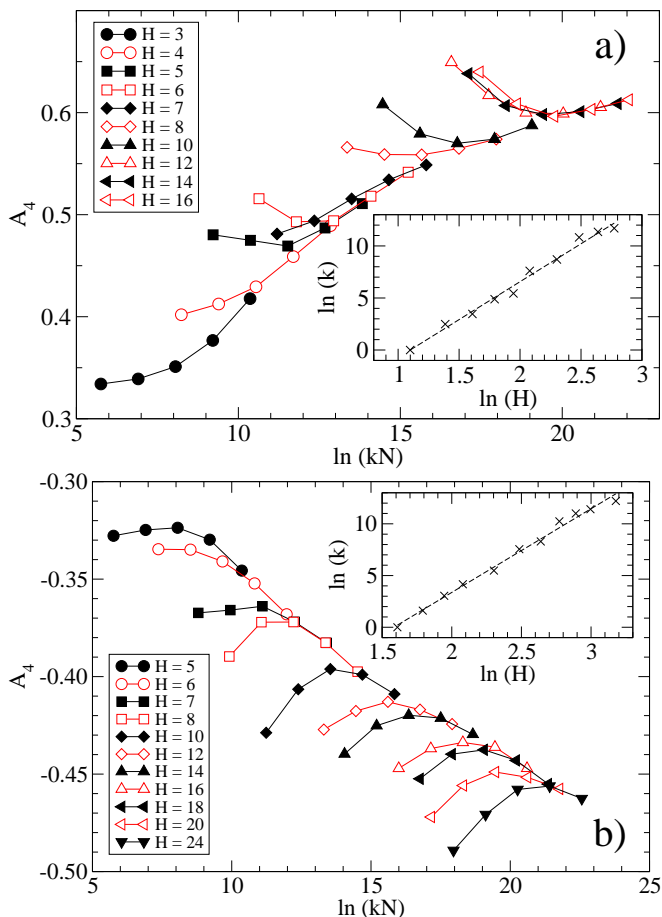


FIG. 4: (Color online) Mastercurves of the evolution of A_4 for **a)** simple cubic and **b)** body-centred cubic growths. These suggest universal approach to respective SC and BCC fixed points. The insets show how the shift factors k applied to N vary with noise reduction parameter H .

tion A_4 to the FCC aggregates, and for comparison A_6 was also evaluated for the BCC and SC clusters. Studies of two-dimensional anisotropic DLA [31] have had some success focussing on the interplay between anisotropy and noise in the growth process, and in this spirit we measured $\sigma(R)/R$, where R is the deposition radius of a cluster and $\sigma(R)$ is the standard deviation of this measurement. This quantity offers a simple measure of fluctuations due to noise during cluster growth; $\sigma(R)/R$ is plotted against A_4 in Figure 7(a) and against A_6 in Figure 7(b) for clusters of each type at various H .

Figure 7(a) shows that for all clusters the noise decreases reasonably monotonically as growth proceeds. SC and BCC growths for all H can be seen to converge towards their respective fixed point values of approximately 0.65 (SC) and -0.5 (BCC). The FCC growths are all grouped around $A_4 \simeq -0.2$, and this plot fails to explain the behaviour of the low H FCC clusters. However, Figure 7(b) gives us an idea of what may be happening: whereas the higher H growths head towards the same final value ($A_6 \simeq 0.5$), the curves for the low H FCC clus-

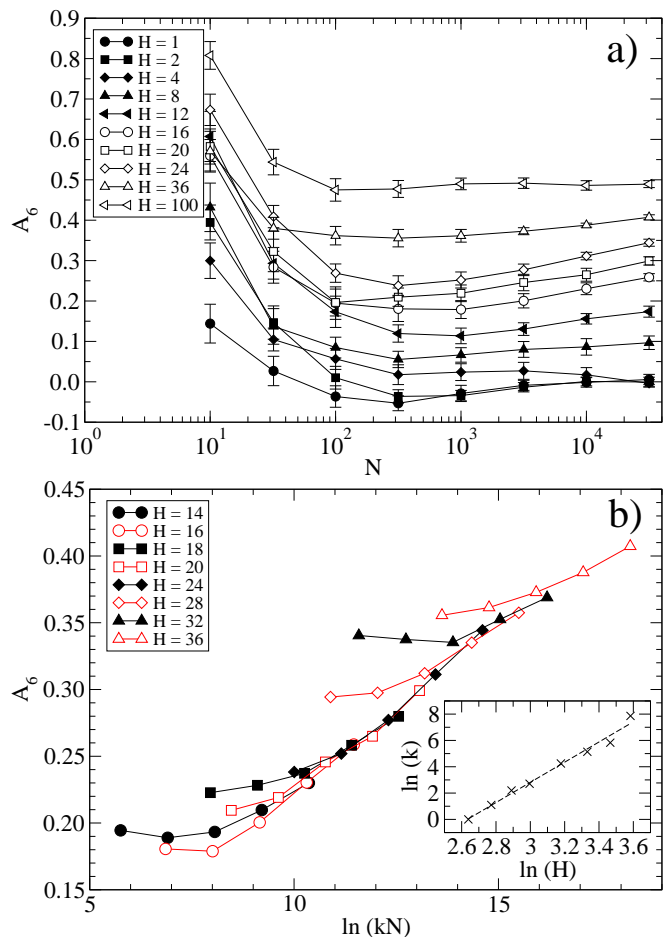


FIG. 5: (Color online) **a)** Anisotropy function A_6 evaluated for FCC growths, based on the average over 10 clusters per curve. Only at higher noise reduction levels is there clear indication that the FCC anisotropy is sustained under growth. **b)** Mastercurve for FCC growths at $H \geq 14$, which do appear to exhibit a common evolution, with the corresponding shift factors inset.

ters have not turned towards this value and appear to be following similar trajectories to the low H BCC clusters. All the SC and BCC clusters appear to be approaching common asymptotic values of A_6 of approximately -0.2 and -0.35 respectively.

Further evidence for this explanation of the FCC cluster behaviour is given by plotting A_4 against A_6 for BCC and FCC growths in Figure 8(a). This clearly shows the BCC clusters evolving (in a direction dependent on H) towards a fixed point. The high H FCC growths also head to their own fixed point, whereas the low H growths are moving in a different direction, towards the BCC fixed point. The inset of Figure 8(a) shows the position of the SC growths in the A_4, A_6 plane; they can also be seen to approach a fixed point from different directions depending on H .

This information allows us to build what we believe to be a consistent picture of the evolution of all three types

of growth, interpreted in terms of how the parameters A_4 and A_6 evolve as a function of increasing lengthscale. This is shown in Figure 8(b). Our anisotropy curves have shown the existence of stable fixed points, for each of SC, BCC and high noise reduction FCC clusters: assuming that the variables A_4 and A_6 capture the key distinction between the different anisotropies studied, these directly imply the three separate stable fixed points shown on Figure 8(b). There is presumably an unstable fixed point located at $(0, 0)$ in the A_4, A_6 plane corresponding to isotropic growth, and the differing trajectories of the FCC clusters dependent on H implies the existence of another unstable fixed point to separate the two behaviours. The measured directions of our data allow us to predict trajectories of growths with different starting points, with flow away from or towards each fixed point depending on its nature.

We next turn our attention to hexagonal growths. We define a parameter $p = \frac{H_z}{H_{xy}}$ where H_z is the number of walker hits required to grow a site in either of the favoured polar directions and H_{xy} is the number of hits required for growth in a favoured planar direction. For all growths $H_{xy} = 100$ while H_z was varied between simulations to give values of p ranging from 0.5 to 4. Low values of p produced column-like growths, while high p resulted in virtually flat aggregates with six arms in the plane. Example clusters are shown in Figure 9.

Aspect ratios of these hexagonal clusters are shown in Figure 10(a). The results are from 5 clusters of size $N = 10^5$ at each value of p , although since a cluster possesses six planar and two polar arms each provides us with twelve measurements of an aspect ratio. Strikingly, the aspect ratios remain almost constant for $N \geq 10^3$, suggesting the existence of a continuous spectrum of fixed points which depend on the input anisotropy. This is contrary to a simple expectation of two fixed points, favouring polar or planar growth respectively.

To investigate this interesting result further we tuned the polar growth of some SC clusters in the same way. Since these clusters possess fewer competing arms than the hexagonal growths, for the same size N they should be more converged towards their asymptotic states. The aspect ratios of these clusters are shown in Figure 10(b), and they appear very similar to the hexagonal results. They do suggest a coherent explanation, however. The $p = 1$ clusters are of course just the standard SC clusters investigated above and since polar and planar lattice directions are in this case equivalent, they unsurprisingly display a constant aspect ratio of 1. This fixed point is presumably stable under growth. The aspect ratios of the extreme cases $p = 0.5$ and $p = 4$ appear to diverge at very large N , suggesting the existence of additional fixed points at infinity and zero, corresponding to column-like or flat growths respectively. The intermediate growths $p = 1.5$ and $p = 2$ approach constant aspect ratios which we interpret to be the fixed point at 1 displaced by the input tuning of the growths. The striking similarity be-

tween these results and those for the hexagonal clusters leads to a similar explanation for their origin.

V. CONCLUSIONS

We have utilised an efficient, dimension-independent numerical implementation of the DLA model to explore the effects of several different lattice anisotropies on three-dimensional aggregates.

For cubic anisotropies we used functions with maxima in the appropriate lattice directions to characterise our aggregates. We have shown that SC and BCC growths approach universal asymptotic states, independent of the level of noise reduction, and that in each case the evolution of the cluster anisotropy can be described by mastercurves.

For face-centred cubic anisotropy, high noise reduction clusters also appear to approach a common asymptotic state. By evaluating the clusters' anisotropic response in the BCC lattice directions we have shown that lower noise reduction FCC growths appear to evolve towards the BCC fixed point. The final appearance of these low noise reduction FCC clusters remains uncertain.

We also studied hexagonal anisotropies with six favoured planar directions and two favoured polar directions. We tuned our growths by varying the criterion for growth in a polar direction, and somewhat surprisingly found that the aspect ratios of our clusters appear to exhibit a continuous spectrum of final states, dependent on the input tuning. These growths bear a striking resemblance to snowcrystal morphologies.

Accurate simulation of real solidification patterns like snowcrystals involves including the effect of a non-constant small-scale cutoff. Theory [15, 16] suggests an equivalence between this and simple dielectric breakdown model growth. A new method of realising DBM growth using random walkers has been implemented in two dimensions [7], and our new code is ideally suited to extending this investigation to three dimensions, of which little or nothing is known. Combining these advances with the anisotropic techniques described above it seems feasible to develop fully self-consistent simulations of dendritic solidification and related phenomena, and work on this task is underway.

Acknowledgments

This research has been supported by the EC under Contract No. HPMF-CT-2000-00800. NRG was supported by an EPSRC CASE award. The computing facilities were provided by the Centre for Scientific Computing of the University of Warwick, with support from the JREI.

-
- [1] T. A. Witten and L. M. Sander, Phys. Rev. Lett. **47**, 1400 (1981).
- [2] M. Plischke and Z. Rácz, Phys. Rev. Lett. **53**, 415 (1984).
- [3] A. Coniglio and M. Zannetti, Physica A **163**, 325 (1990).
- [4] E. Somfai, L. M. Sander, and R. C. Ball, Phys. Rev. Lett. **83**, 5523 (1999).
- [5] C. Amitrano, Phys. Rev. A **39**, 6618 (1989).
- [6] M. H. Jensen, J. Mathiesen, and I. Procaccia, Phys. Rev. E **67**, 042402 (2003).
- [7] E. Somfai, N. R. Gould, R. C. Ball, J. P. Devita, and L. M. Sander, Phys. Rev. E **70**, 051403 (2004).
- [8] J. S. Langer, Rev. Mod. Phys. **52**, 1 (1980).
- [9] W. W. Mullins and R. F. Sekerka, J. Appl. Phys. **34**, 323 (1963).
- [10] J. Nittmann, G. Daccord, and H. E. Stanley, Nature **314**, 141 (1985).
- [11] M. Matsushita, M. Sano, Y. Hayakawa, H. Honjo, and Y. Sawada, Phys. Rev. Lett. **53**, 286 (1984).
- [12] R. M. Brady and R. C. Ball, Nature **309**, 225 (1984).
- [13] L. Niemeyer, L. Pietronero, and H. J. Wiesmann, Phys. Rev. Lett. **52**, 1033 (1984).
- [14] J. Nittman and H. E. Stanley, J. Phys. A: Math. Gen. **20**, L1185 (1987).
- [15] R. C. Ball and E. Somfai, Phys. Rev. Lett. **89**, 135503 (2002).
- [16] R. C. Ball and E. Somfai, Phys. Rev. E **67**, 021401 (2003).
- [17] K. G. Libbrecht and V. M. Tanusheva, Phys. Rev. E **59**, 3253 (1999).
- [18] S. C. Huang and M. E. Glicksman, Acta. Metall. **29**, 717 (1981).
- [19] D. P. Corrigan, M. B. Koss, J. C. LaCombe, K. D. de Jager, L. A. Tennenhouse, and M. E. Glicksman, Phys. Rev. E **60**, 7217 (1999).
- [20] W. B. Russel, P. M. Chaikin, J. Zhu, M. V. Meyer, and R. Rogers, Langmuir **13**, 3871 (1997).
- [21] J. Zhu, M. Li, R. Rogers, W. Meyer, R. H. Ottewill, W. B. Russel, and P. M. Chaikin, Nature **387**, 883 (1997).
- [22] M. E. Glicksman and S. P. Marsh, in *Handbook of Crystal Growth*, edited by D. T. J. Hurle (Elsevier, Amsterdam, 1993), p. 1077.
- [23] R. Kobayashi, Physica D **63**, 410 (1993).
- [24] W. L. George and J. A. Warren, J. Comp. Phys. **177**, 264 (2002).
- [25] P. Meakin, Phys. Rev. A **36**, 332 (1987).
- [26] R. C. Ball, R. M. Brady, G. Rossi, and B. R. Thompson, Phys. Rev. Lett. **55**, 1406 (1985).
- [27] R. C. Ball and R. M. Brady, J. Phys. A **18**, L809 (1985).
- [28] S. Tolman and P. Meakin, Phys. Rev. A **40**, 428 (1989).
- [29] N. E. Bowler and R. C. Ball (2004), cond-mat/0404650.
- [30] R. C. Ball, N. E. Bowler, L. M. Sander, and E. Somfai, Phys. Rev. E **66**, 026109 (2002).
- [31] P. W. Barker and R. C. Ball, Phys. Rev. A **42**, R6289 (1990).

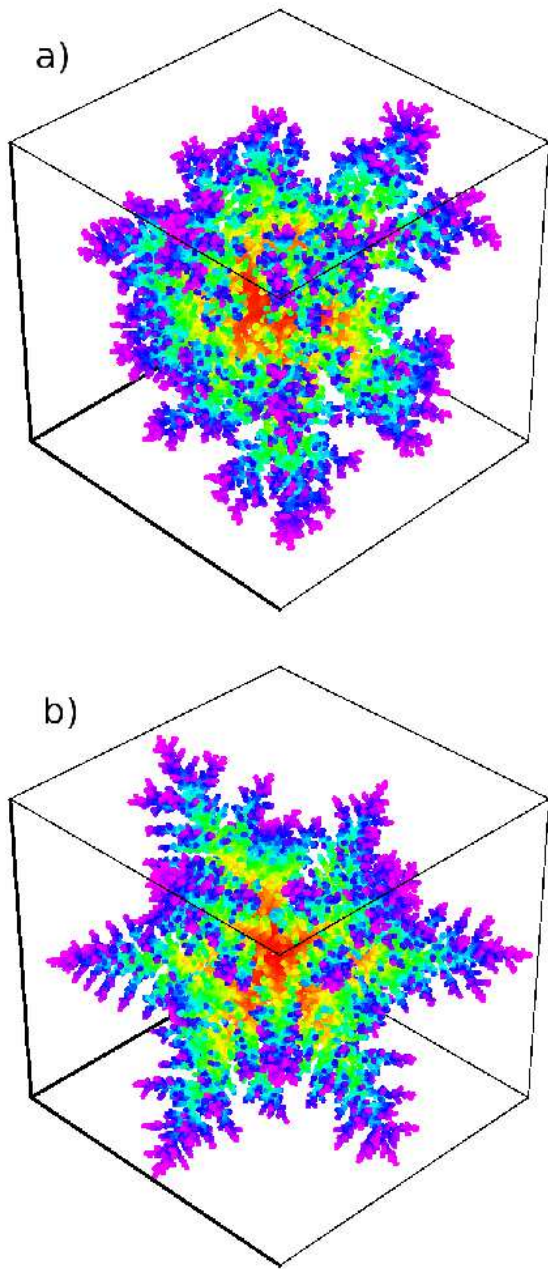


FIG. 6: (Color online) FCC clusters grown by the new method: **a)** low noise reduction $H = 6$, and **b)** high noise reduction $H = 100$. Both clusters contain 3.16×10^4 sites grown. The low noise reduction case appears to show some growth bias to the BCC lattice directions (corners) as per BCC lattice growth in Figure 2. The high noise reduction cluster exhibits growth in all twelve FCC lattice directions, which correspond to the mid-edges of the box drawn.

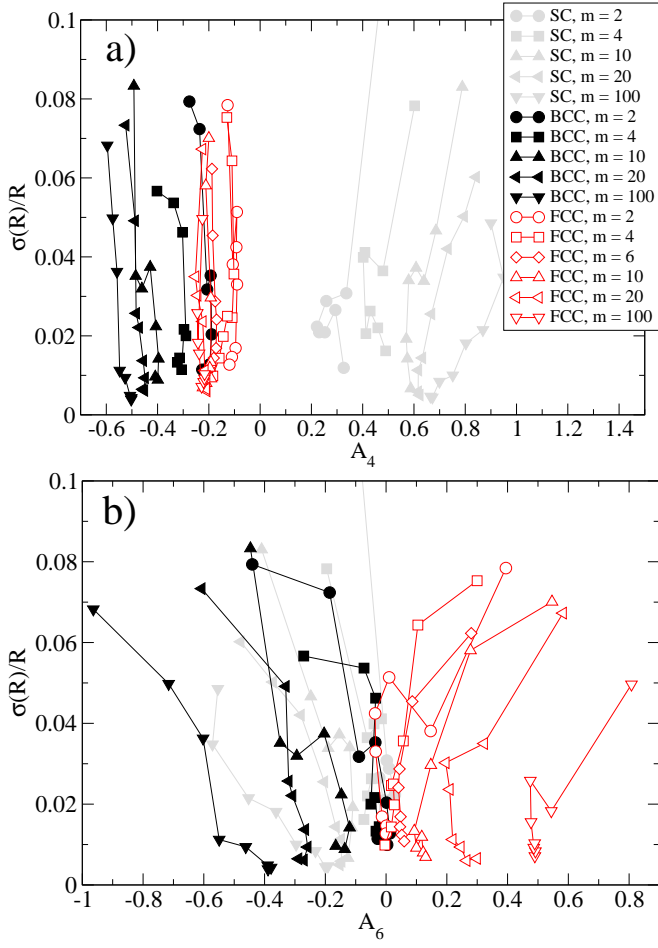


FIG. 7: (Color online) The relative fluctuation in cluster radius (at fixed N), plotted against each of the anisotropy measures A_4 and A_6 as clusters grow. Increasing N corresponds to moving generally downwards in these plots, and the symbols are the same on both panels.

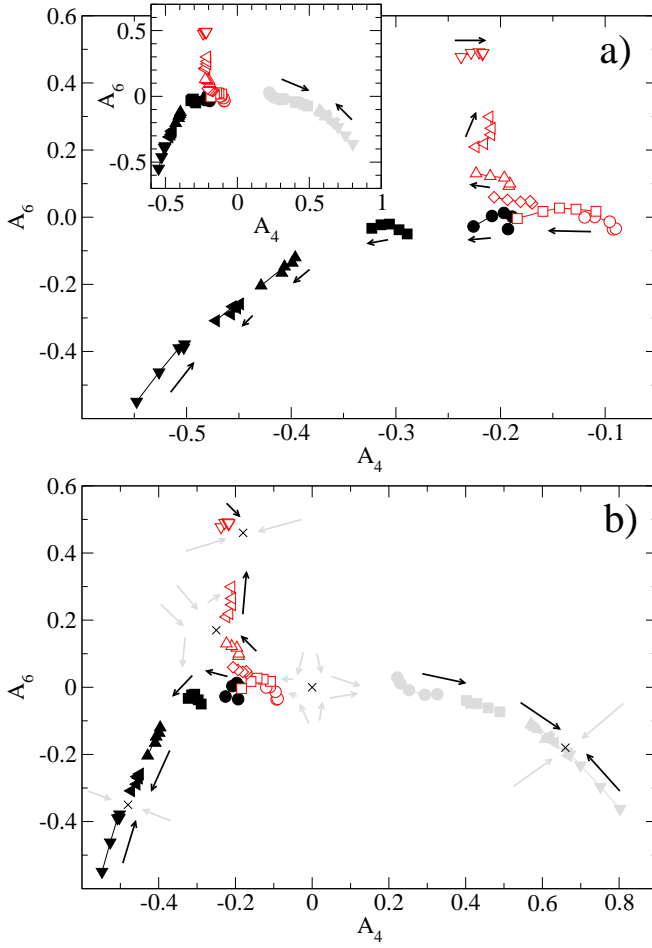


FIG. 8: (Color online) **a)** The evolution of clusters in the plane of A_4 and A_6 for BCC and FCC clusters at various noise reduction levels (always averaging over samples of 10), with arrows to indicate the direction of trajectories. The inset shows the well separated evolution of SC clusters in the same plane. **b)** The same data can be interpreted as renormalisation flows for how effective parameters evolve as a function of lengthscale, leading to the inferred fixed points shown (crosses). It is an assumption here that the lowest relevant angular harmonics A_4 , A_6 do capture the key distinction between the three different applied anisotropies. Bold arrows show observed evolution whereas gray arrows show the presumed flow from other starting points. The symbols on both panels are the same as those in Figure 7.

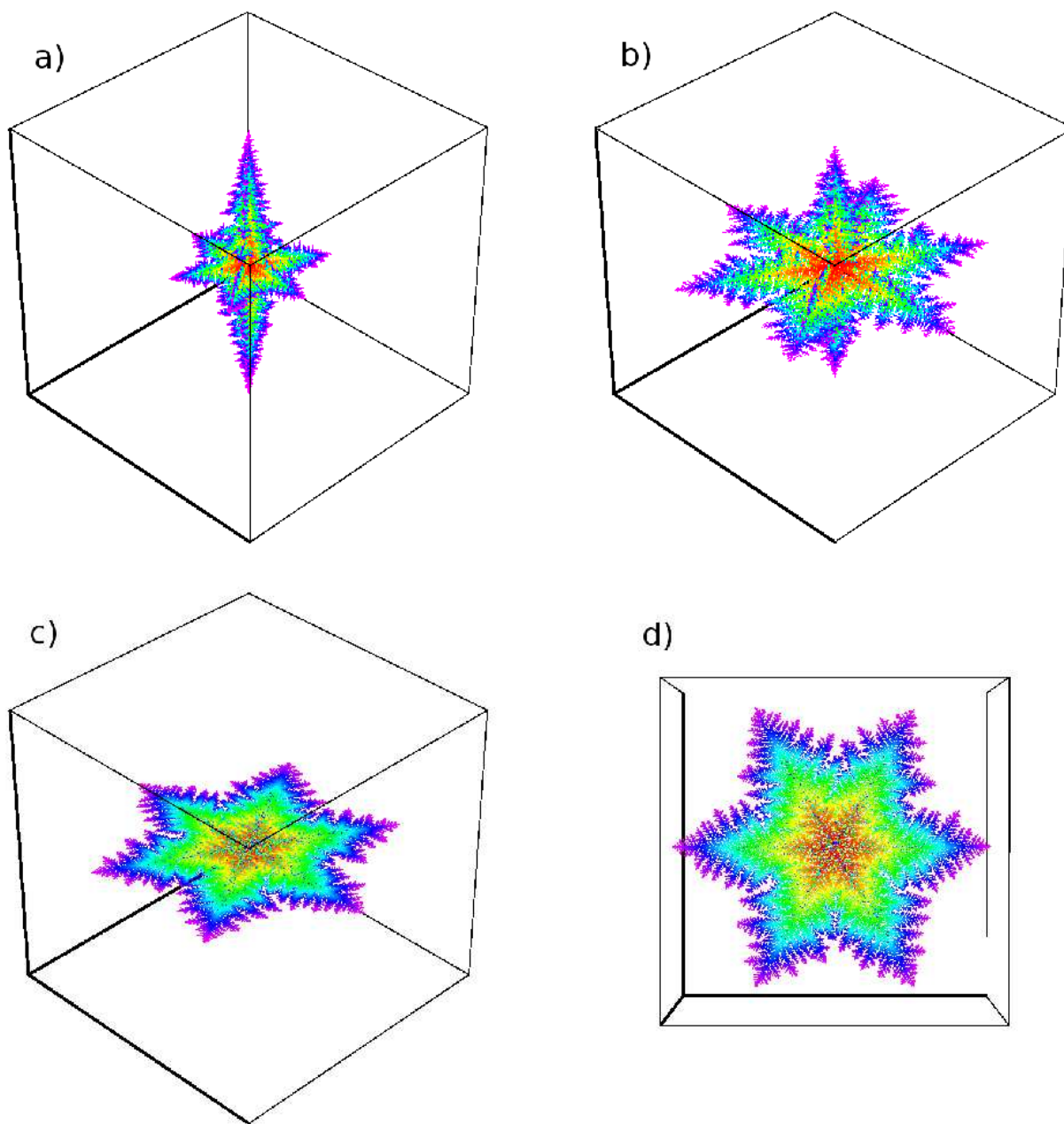


FIG. 9: (Color online) Clusters grown favouring six planar directions and two polar directions. The parameter p is a measure of the relative ease of planar growth compared with polar, with high values of p favouring planar growth. Shown are **a)** $p = 1$, **b)** $p = 1.5$, and **c)** $p = 4$; **d)** shows the $p = 4$ cluster viewed from above, highlighting the complex six-armed morphology of these growths.

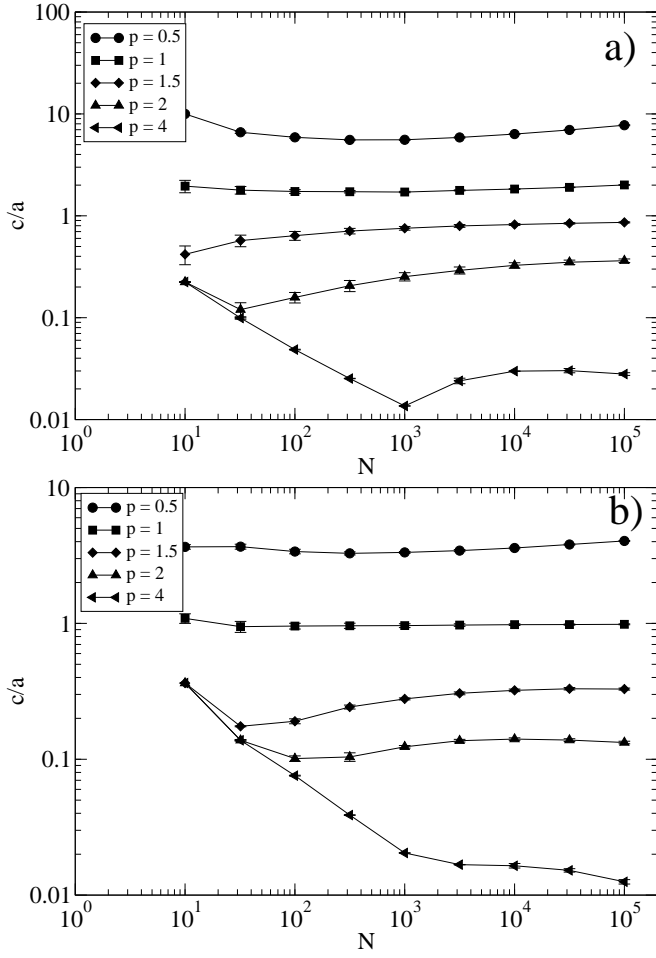


FIG. 10: Aspect ratios of **a)** hexagonal growths, and **b)** SC growths, both with tunable input polar anisotropy p . The data is from 5 clusters of each type for each value of p ; using both polar arms and the 6 (hexagonal) or 4 (SC) planar arms each cluster provides 12 or 8 measurements, respectively, of an aspect ratio at size N .